1. Introduction

In Hawai‘i, floods contributed to the largest economic loss and the second largest cause of death from natural hazards between 1996 and 2018 (Data sources: hazards reported from the Storm Event Database (National Centers for Environmental Information (NCEI), 2019a). Flooding is associated with erosion that scours stream beds, abrades bedrock, and moves large amounts of sediment and debris downstream, and downcutting channels. Improving our understanding of changes in flooding will inform watershed planning and develop potential mitigation strategies, especially as climate warming continues to alter precipitation patterns and hydrological processes. In theory, increasing global temperature results in increased water vapor in the air with its greater water holding capacity that lead to larger and more frequent extreme precipitation events (Held et al., 2006; Knutson and Manabe, 1995). Extreme precipitation events have increased in magnitude and frequency with warming temperature in many regions (Alexander et al., 2006; Beck et al., 2015; Donat et al., 2013; Easterling et al., 2017; Groisman et al., 2005; Wentz et al., 2007; Westra et al., 2013). Nevertheless, an analysis using 390 watersheds across the U.S. found the 99th percentile precipitation does not totally contribute to 99th percentile streamflow, and the contributions varied with soil moisture condition (Ivancic and Shaw, 2015). Unlike rainfall, streamflow and flooding are scale-dependent based on local watershed characteristics (Wasko and Sharma, 2017). Therefore, extreme rainfall trends might not fully describe the observed patterns in extreme streamflow trends, and their linkage needs to be studied locally.

Previous studies have shown various trends in extreme streamflow across the world, such as in North America (Cunderlik and Ouarda, 2009; Groisman et al., 2001), Europe (Blöschl et al., 2019; Hannaford and Marsh, 2008; Mediero et al., 2014; Renard et al., 2008), and Australia (Ishak et al., 2013; Zhang et al., 2016). The annual maximum peak flow in Canada decreased (Cunderlik and Ouarda,2009), whereas the high discharge in the eastern U.S. increased (Groisman et al., 2001). In Europe, the annual 10-day streamflow and annual maximum peak flow between 1969 and 2003 in the U.K. increased (Hannaford and Marsh, 2008), but decreased in France between 1968 and 1998 (Renard, 2008). The magnitude and frequency of annual peak flow in Spain generally decreased from 1942 to 2009 (Mediero et al., 2014). In Australia, the annual peak flow decreased in the sourth but increased in the north (Ishak et al., 2013; Zhang et al., 2016).In addition to changes in the frequency and duration of extreme streamflow events, the timing of flooding has also shifted in Europe, including earlier spring snowmelt floods in northern areas, later winter floods along the Mediterranean coast, and earlier winter floods in western Europe (Blöschl et al., 2017). As trends in extreme streamflow are geographically heterogeneous, it is critical to study the trends of extreme streamflow locally. Most trend analyses of extreme streamflow events have been conducted in continental systems, and little has been discussed in tropical regions, which are sensitive to changes in large climate patterns.

Extreme events in the tropics, including Hawai‘i, are influenced by large-scale climate variability, including the El Niño-Southern Oscillation (ENSO), the Pacific Decadal Oscillation (PDO), and the Pacific North America teleconnection pattern (PNA) (Beck et al., 2015; Chu et al., 1993; Chu and Chen, 2005; Elison Timm et al., 2011; Lyons, 1982; Mantua et al., 1997). Recent evidence indicates that climate change has affected the ENSO’s behavior across the tropics (Diaz and Giambelluca, 2012; O’Connor et al., 2015; Trenberth and Hoar, 1997) and changed El Niño properties, including its earlier starting time (Wang et al., 2019). In Singapore, both daily and hourly maximum rainfall were found to increase between 1981 and 2010 with ENSO-related changes in their intensity and timing (Beck et al., 2015). With global warming, the intensity and longevity of tropical cyclones (TCs) in the Northeast Pacific has slightly decreased between 1986 and 2005 (Klotzbach, 2006); however, the frequency of TCs around the Pacific are expected to occur more frequently in the future (Li et al., 2010; Murakami et al., 2013).

In Hawai‘i, there are two seasons, dry (May – Sep.) and wet (Oct. – Apr.) seasons. In the dry season, an extreme precipitation is often attributed to hurricanes or TCs (e.g., Nugent et al., 2020). The TC activity is more favorable under El Niño conditions (Chu and Wang, 1997; Jin et al., 2014) and associates with the Western North Pacific (WNP) biennial oscillations (Luo et al., 2020). In the wet season, winter storms contribute the most to extreme rainfall. A combination of PNA, ENSO, and PDO contributes to the rainfall variability in the wet season (Frazier et al., 2017). During El Niño conditions, the wet season months often become drier in Hawai‘i and wetter during La Niña conditions. In addition, negative periods of PDO that align with La Niña, typically strengthen the intensity, and lengthen the wetter period (Chen and Chu, 2014). Streams in Hawai‘i respond to rainfall rapidly (within hours), as majority of streams are first order streams with small drainage areas, steep slopes, and short time of concentration. The low-permeable volcanic geology of all islands combined with high intensity rainfall simultaneously produces runoff, generating flashy hydrographs (Oki, 2003). Besides, the coastal areas of Hawaiian watersheds are oftenurbanized with impervious surface and channelized streams, which contribute to the fast raising and falling hydrograph. In Hawai‘i, we expect extreme streamflow to highly correspond to its rainfall.

Although we anticipate a close relationship between extreme streamflow and rainfall in Hawai‘i, previous studies investigated their trends separately. Chu et al. (2010) and Chen and Chu (2014) showed that extreme precipitation between the 1950s and 2007 became more common on the largest island, Hawai‘i Island, but not on other islands, with the indices of the annual count of days when the precipitation over 25.4 mm, annual maximum consecutive 5-day precipitation, and the normalized 95th percentile precipitation. Bassiouni and Oki (2013) investigated streamflow trends in Hawai‘i and found that 16 out of 26 gauges of peak flow decreased between 1943 and 2008. Furthermore, Clilverd et al. (2019) assessed streamflow records for 23 unregulated streams from 1967 to 2016 across the Hawaiian Islands and found significant declines in baseflow and surface runoff. They also discovered significant declines in peak flow on Hawai‘i Island. However, in some cases, peak flow showed opposite trends from extreme precipitation (e.g., Chen and Chu, 2014; Chu et al., 2010; Clilverd et al., 2019). Because extreme rainfall and streamflow trends have been investigated separately, the linkages between these extreme events are not clear. To better understand their associations, we need a joined examination of extreme rainfall and peak flow trends.

This study aims to characterize local changes in the annual maximum daily rainfall (RF_{max}) and the annual peak flow (PF_{max}) by examining their spatial and temporal trends with their associations across five major Hawaiian Islands. We investigated the trends in RF_{max} and PF_{max} to determine possible relationships between the meteorological and hydrologic response to climate change, by studying: 1) the spatial distribution of trends in RF_{max} and PF_{max} in Hawai‘i from 1970 to 2005; 2) the association between peak rainfall and peak flow by pairing representative rain gauges to crest gauges; and 3) the temporal shifts of RF_{max} and PF_{max}, respectively.

2. Materials and methods

2.1 Study area

Among the eight major Islands, we focus on the five largest islands, from west to east, Kaua‘i, O‘ahu, Moloka‘i, Maui, and Hawai‘i Island, spanning from 18.9°N, 154.8°W to 22.24°N, 159.8°W, where have most and long-term rainfall and peak flow records. The climate in Hawai‘i is strongly affected by the Hadley cell atmospheric circulation patterns in the Pacific. These patterns generate the typical northeast trade winds in the northern hemisphere, which induces orographic rainfall when moist air encounters the steep island topography (Lyons, 1982). Thus, these islands' windward facing sides experience more frequent rain and higher annual rainfall below trade wind inversion (TWI; approximate mean elevation at 2,000 m; Cao et al. 2007), while the leeward sides are much drier. In addition, widespread and intense precipitation may be attributed to four other types of atmosphere conditions – (i) Kona storms, the low-pressure systems that usually develop on the west of the islands accompanied with southern winds, (ii) cold fronts, (iii) upper-level trough, or (iv) tropical cyclones (Caruso and Businger, 2006; Kodama and Barnes, 1997). The wide range of terrain across the Hawaiian Islands with the large scale atmospheric systems results in highly heterogeneous climate patterns, and therefore steep rainfall gradients (mean annual rainfall from 200 mm to 10,000 mm; Giambelluca et al., 2013). Further, watersheds in Hawai‘i are typically characterized by young volcanic geology, small drainage size, steep topography, and limited channel storage (Craig, 2003). Thus, streams frequently experience flash flooding where water levels rise and fall rapidly within hours of locally intense rainfall events (Oki, 2003; Sahoo et al., 2006).

2.2 Data

The locations of rain and crest (annual peak flow) gauges across the Hawaiian Islands and their physiographical regions (windward vs. leeward) are shown in Figure 1. We sought crest gauges with the longest period of record and greatest overlap with rainfall records, which resulted in a study period of 1970 to 2005 (by water year). Daily rainfall data were obtained from the National Centers for Environmental Information (NCEI) and the U.S. Geological Survey (USGS). Eighty-four rain gauges (Kaua‘i, n=17; O‘ahu, n=25; Moloka‘i, n=3; Maui, n=20, and Hawai‘i Island, n=19), with data records longer than half of the study period, were used in this study (Figure 1). Most rain gauges were located at low elevations and only a few were above the average TWI (> 2,000 m). The rain gauges were not evenly distributed across the islands, except for Kaua‘i. For O‘ahu and Moloka‘i, most of rain gauges were located on the leeward side, whereas for Maui and Hawaii island, rain gauges were located mostly on the windward side and along the coast. Annual records of peak flow were obtained for 111 long-term crest gauges (circles in Figure 1; Kaua‘i, n=18; O‘ahu, n=45; Moloka‘i, n=7; Maui, n=25, and Hawai‘i Island, n=16) from the water years 1970 to 2005, maintained by the USGS. Compared with the distribution of rain gauges, crest gauges have a more even spatial distribution, except on Hawai‘i Island, wherecrest gauges were predominantly located on the windward side. Peak flow values of each gauge were standardized by the watershed area and converted to a daily scale (mm/day) that is comparable to the daily rainfall values (mm/day).

We used two climate indices to examine shifts in the seasonality of peak events, the Oceanic Niño Index (ONI) and the Pacific Decadal Oscillation (PDO) index. The ONI is one of the primary indices for monitoring ENSO. It is calculated by averaging sea surface temperature monthly anomalies of the east-central equatorial Pacific Ocean, Niño-3.4 region. We retrieved monthly ONI from the Climate Prediction Center (CPC) (2019). The PDO index is defined by ocean temperature anomalies in the northeast and the tropical Pacific Ocean. The PDO index is downloaded from NCEI (2019b).

2.3 Trend analysis

Trends in the magnitude of RF_{max} and PF_{max} were analyzed using the non-parametric Mann-Kendall test (Hirsch and Slack, 1984; Mann, 1945); a p-value < 0.05 was used to indicate the significant trends. Changes of the magnitude were evaluated using Sen's slope (Sen, 1968). Then, the change of values per year were divided by the mean value of the study period to generate percent change in the value per year. These two trend analysis methods are recommended for analyzing environmental time series data that are not normally distributed, with no data distribution assumptions required (Hirsch and Slack, 1984; Mann, 1945). Additionally, evaluation with Sen's slope is not sensitive to outliers. These trend analyses have been widely applied to quantifying and testing the significance of streamflow trend (Bassiouni and Oki, 2013; Clilverd et al., 2019; Oki, 2004; Small et al., 2006) and rainfall (Chen and Chu, 2014; Frazier and Giambelluca, 2016). The R package, 'trends' (Pohlert et al., 2018), was applied in this analysis.

2.4 Analysis of paired rainfall gauges and stream crest gauges

In addition to examining data from 84 rain gauges and 111 crest gauges, we paired crest gauges with rain gauges that most likely represent the rainfall received from upstream watersheds to better understand the associations between rainfall and peak flow. We paired them geographically with following criteria, ranked in order of preference:

1) The rain gauge was located upstream of the crest gauge in the same watershed; if multiple rain gauges existed in the same watershed, we chose the gauge with the highest elevation but below the TWI.
2) The rain gauge was upstream from the crest gauge in the neighboring watershed.
3) The rain gauge was close to the crest gauge (within a 5 km radius).
4) The rain gauge best represented the rainfall of the upstream watershed of the crest gauge, despite being in different watersheds. For example, three crest gauges on the windward side of East Maui were paired with one rainfall gauge at Hana, Maui, that represents the windward rainfall.

Subsequently, we extracted daily rainfall on the same day of the PF_{max} of these paired gauges. Additionally, 2-day and 5-day accumulated rainfall were examined to consider antecedent conditions and rainfall events that lasted more than one day.

2.5 Examination of temporal shifts in annual maximum rainfall and peak flow

We examined the temporal shifts of RF_{max} and PF_{max} with circular statistics (Zar, 1999) by using the R package, "circular" (Lund et al., 2017). Circular statistics is powerful when applying to the data with unit radius or degree on a circumference (Pewsey et al., 2013). We applied a circular analysis to the occurrence time of RF_{max} and PF_{max} for the study period by converting the occurrence date (d_y) of RF_{max} and PF_{max} into angular values for each year, y:

$$\vartheta_y = 2\pi * \frac{d_y}{D_y} \qquad 0 \le \vartheta_y \le 2\pi \qquad \text{Eq. 1}$$

Where $d_y = 1$ corresponds to January 1st and $d_y = D_y$ to December 31st with D_y is the number of days in that year (i.e., 365 or 366). Then, the Sen's slope, z, is adjusted for estimating trends in the timing:

$$z = median\left(\frac{\vartheta_j - \vartheta_i + c}{j - i}\right) \quad with\ c = \begin{cases} -\pi & if\ \vartheta_j - \vartheta_i > \pi \\ \pi & if\ \vartheta_j - \vartheta_i < -\pi \\ 0 & otherwise \end{cases} \qquad \text{Eq. 2}$$

Where i and j indicate the year covering all possible pairs of years within the study period, and $i < j$. The adjustment factor, c, aims to represent the shifting trend (i.e., to earlier or later) based on the occurrence time at the ith year, when the differences between ϑ_i and ϑ_j are larger than π. Finally, we analyzed the temporal shifts by different physiographic zones (i.e., windward and leeward), to examine the effects of different rainfall forming mechanisms.

3. Results

3.1 Changes in maximum rainfall magnitudes

Out of 84 rain gauges, the majority (67%) of rain gauges exhibited decreasing RF_{max} magnitude (Kaua‘i, n=9; O‘ahu, n=19; Moloka‘i, n=1; Maui, n=15, and Hawai‘i Island, n=12). The magnitude of RF_{max} significantly decreased at seven rain gauges: one on O‘ahu ($p = 0.021$; changed – 1.5% per year; mean = 195.2 mm), five on Maui ($p < 0.01$; changed from −2% to −4%; mean: 22.5 mm to 70 mm), and one on Hawai‘i Island ($p = 0.046$; changed −1.6%; mean = 171.6 mm) (Figure 2). The remaining 33% of rain gauges showed increasing RF_{max} trends (Kaua‘i, n=8; O‘ahu, n=6; Moloka‘i, n=2; Maui, n=5, and Hawai‘i Island, n=7) (Figure 2). Significant increasing trends only occurred at one gauge on Hawai‘i Island ($p = 0.047$) and changed 2.7% per year with a mean of 151.4 mm. On Kaua‘i, increasing RF_{max} trends were primarily located on the windward side, whereas there were no discernable differences in RF_{max} between leeward and windward on the other islands. Decreasing trends in RF_{max} dominated on Oahu, Maui, and Hawai‘i Island, while no particular trend direction prevailed on Kauai and Moloka‘i. However, there are too few rain gauges on Moloka‘i to address the spatial distribution in RF_{max} trends.

3.2 Changes in peak flow magnitudes

Decreasing magnitude in PF_{max} occurred at 60% of the crest gauges (Kaua‘i, n=8; O‘ahu, n=29; Moloka‘i, n=3; Maui, n=16, and Hawai‘i, n=11), predominantly on O‘ahu, Maui, and Hawai‘i islands (Figure 3). Statistically significant decreasing trends occurred at a single gauge on O‘ahu ($p < 0.002$; decreased 6.5%; mean = 195.8 mm/day) and two on Maui ($p < 0.011$; decreased 4.2%; means = 224.8 mm/day and 107.8 mm/day, respectively). Although decreasing PF_{max} trends dominated across O‘ahu, some crest gauges still showed increasing trends, with two statistically significant ($p < 0.05$) peak flow trends that rose 5.8% and 3.4% with means of 302 mm/day and 80 mm/day, respectively. There was a general pattern of increasing PF_{max} on the windward sides of Kaua‘i, Moloka‘i, and East Maui (Figure 3). Compared with RF_{max}, PF_{max} shows a greater physiographic division (i.e., windward and leeward) in trend directions.

3.3 Associations between peak flow, annual maximum rainfall and paired rainfall

When pairing rainfall and crest gauges, there are 18 pairs identified following the first criterion, and there are nine, eight, and four pairs found in the subsequent criteria, respectively. This resulted in a total of 39 pairs across islands (2 on Kaua‘i, 15 on O‘ahu, 1 on Moloka‘i, 14 on Maui, and 17 on Hawai‘i Island). Some rain gauges were paired with multiple crest gauges as they were the most representative rainfall of the given watersheds of crest gauges. This applied at 13 crest gauges on Oʻahu (5 at Poamoho, 2 at Waiāhole, 4 at Pauoa Flats, 2 at Palolo valley); seven crest gauges on Maui (4 at Haleakala and 3 at Hana); and at four crest gauges on Hawaiʻi Island (2 at Waiakea and 2 at Mauna Kea) (Figure 4).

The timing of RF_{max} rarely coincided with the timing of PF_{max}. Out of the 39 pairs of rainfall and crest gauges, almost half (46%) of the pairs have different trend directions between RF_{max} and PF_{max} (Figure 4). Within the study period, when we extracted the same date rainfall with PF_{max}, 67% of the paired rainfall and PF_{max} records had consistent trends (increasing or decreasing). However, when we extracted the 2-day and 5-day accumulated rainfall with PF_{max}, the percent of consistency decrease (Table 1).

Among the pairs having consistent trends, 56% of them showed decreasing trends, whereas the remaining 44% exhibited increasing trends (Figure 4). There was no clear leeward versus windward patterns in trend direction across the islands. Paired decreasing trends occurred on both windward and leeward sides of Oʻahu and Maui, and on windward Hawaiʻi Island. Consistent increasing trends occurred on the leeward side of Oʻahu, windward side of Maui, and north of Hawaiʻi Island.

3.4 Changes in the timing of annual maximum rainfall and peak flow

RF_{max} and PF_{max} often occurred during the wet season (Oct. – Apr.) with the median occurrence time of RF_{max} in earlier January and the median occurrence time of PF_{max} in mid-January for all gauges during the study period (Figure 5a, b). From 1970 to 2005, the occurrence time of both RF_{max} and PF_{max} shifted to an earlier time in the wet season, from late January to late December (Figure 5c, d). Yet, the occurrence time oscillated between earlier and later throughout the four sub-periods (Figure 5c, d). The Sen's slope statistics also supported the temporal shifts in the study period. The Sen's slope estimator for the timing of the RF_{max} and the PF_{max} were $-1.34°$ (~ 1.5 days earlier) and $-1.24°$ (~ 1.5 days earlier with p-value < 0.05) in leeward regions, respectively; $-0.404°$ (~ half day with p-value < 0.05) and 0.231° (~ 6 hours later with p-value < 0.05) in windward areas, respectively.

3.5 The relationships of annual maximum rainfall and peak flow to large-scale climate variability

The magnitude of RF_{max} and PF_{max} showed no clear relationships to either the strength of ENSO (**Error! Reference source not found.**) or PDO (**Error! Reference source not found.**) indices. On the other hand, the median occurrence times of both RF_{max} and PF_{max} shifted earlier with a two to seven years cycle, regardless in windward or leeward areas (Figure 6 and 7), which were correlated to the cycle of ENSO. Specifically, the median occurrence times of RF_{max} and PF_{max} shifted to earlier during warm phase of ENSO (shaded in red in Figures 6 and 7). The ENSO's impact on median occurrence times was more pronounced in leeward regions, i.e., with 12(8) recognized El Niño(La Niña) events, 9(5) RF_{max} and 9(6) PF_{max} occurred earlier(later) in a water year (Figure 6). However, there is no correlation between the strength of ENSO (i.e., higher values of index) and the amount of shifting in occurrence times of RF_{max} and PF_{max}, with a correlation coefficient -0.15. Besides, the magnitude and occurrence time of RF_{max} and PF_{max} were not directly correlated to PDO (Figure B2).

4. Discussion

4.1 Overview

Changes in the extreme events are driven by complex atmospheric conditions and antecedent hydrological conditions, and it is unclear whether observed changes in rainfall and streamflow are due to natural atmospheric variability or global warming. Climate models have projected more intense rainfall under a warming climate and led to more severe flooding (Trenberth, 2011). The dataset presented here extends our knowledge of changes in both magnitude and occurrence time of RF_{max} and PF_{max} and their relationships to physiography and atmospheric circulation across the Hawaiian Islands. We analyzed temporal and spatial trends in RF_{max} and PF_{max}, examined the association between RF_{max} and PF_{max}, and inspected the temporal shifts of RF_{max} and PF_{max}. Five key findings of this study were: 1) decreasing RF_{max} trends in more than half of gauges, particularly on O‘ahu and Maui; 2) decreasing PF_{max} trends in most gauges on O‘ahu, Maui and Hawai‘i Island, and more physiographic patterns in PF_{max} trends than RF_{max} trends; 3) different timing between the PF_{max} and the RF_{max}; 4) shifting in the occurrence times of RF_{max} and PF_{max} to earlier, except for PF_{max} in windward areas, and 5) an effect of ENSO on the occurrence time of RF_{max} and PF_{max}. Our results highlight that changes in RF_{max} are not sufficient to explain the observed trends in PF_{max}. In addition, the observed shifts in the occurrence time of RF_{max} and PF_{max} are important for flood risk and environmental management.

4.2 Comparing trends in the Hawaiian Islands to other studies

The predominantly decreasing trends of RF_{max} and PF_{max} shown in this study are consistent with previous findings in Hawai‘i (Bassiouni and Oki, 2013; Chu et al., 2010; Clilverd et al., 2019). However, we did not find increasing RF_{max} trends on Hawai‘i Island as suggested by Chu et al. (2010). This difference may be in part due to the differences in the examined period (1970-2005 vs. 1950-2007), and it highlights cautiously using fixed periods of record as statistical significances of long-term trends (Frazier and Giambelluca, 2016). The majority of PF_{max} stations showed declining trends across the state of Hawai‘i during our study period, particularly on O‘ahu and Hawai‘i Island. Changes in the magnitude of PF_{max} range from –6.5% to 5.8% per year.

In general, the Hawaiian Islands are experiencing decreasing RF_{max} and PF_{max}, whereas extreme rainfall has increased in some continental regions globally (Changnon and Kunkep, 1995; Groisman et al., 2004; Hannaford and Marsh, 2008; Lins and Slack, 1999; Petrow and Merz, 2009). Madsen et al. (2014) indicated the trends of extreme precipitation and floods in Europe are heterogeneous. Beside regional factor, trends of extreme hydrological events may vary due to different definitions or methodologies to detect the trend, e.g., the maximum value over a period, count of precipitation days over a threshold, the percentile values, frequency, etc. (Cunderlik and Ouarda, 2009; Do et al., 2017; Douglas et al., 2000; Hannaford and Marsh, 2008; Ishak et al., 2013; Lins and Slack, 1999; Madsen et al., 2014; Petrow and Merz, 2009). Further, variation in the observed peak flow trends may be due to different causes or mechanisms that generate peak flow, such as intense rainfall, saturated soil, or snow melt (Blöschl et al., 2017; Cunderlik and Ouarda, 2009). Studies in tropical regions (i.e., Singapore (Beck et al., 2015) and India (Pingale et al., 2014)) only showed an increase in annual maximum daily precipitation but little has been done in examining the changes of peak flow and in other tropical islands. In Hawai‘i, decreasing PF_{max} may be related to decreased RF_{max}; however, little research has examined higher temporal resolution (i.e., subdaily) rainfall and its changes. Subdaily rainfall could better associate with peak flow as streamflow responds to rainfall within hours in Hawaiʻi streams. In addition, the currently increasing drought condition across the Hawaiian Islands (Frazier et al., 2019) may also contribute to decreasing PF_{max} (decreasing the opportunity of saturation excess overland flow). This study adds to the knowledge of peak flow changes in tropical regions, especially on those tropical islands that are often frontline to the impact of changing climate and are likely vulnerable to the change in the precipitation patterns. Nevertheless, further studies with long-term data recording of peak flows and high-resolution rainfall will assist future assessments of their relationships and the mechanisms driving the observed across the islands.

4.3 The inconsistency between annual peak flow and paired rainfall trends

We found that PF_{max} rarely occurred at the same time as or soon after RF_{max}, and only 64% of paired gauges showed consistent trend directions between daily rainfall and the peak flow. The pairs with inconsistent trends may be an artifact of the limited availability of paired rain gauges, as pairs showing inconsistent tends were mainly located in different watersheds or sub-watersheds to each other. However, some of the inconsistency cannot be explained by the spatial mismatch, for example, the Poamoho rain gauge on Oʻahu best represented the rainfall on Koʻolau Mountain for nearby watersheds, but interestingly three out of four nearby crest gauges were inconsistent with its rainfall trend. The inconsistency between PF_{max} and the paired rainfall may be due to that rainfall does not always lead to the peak flow, and additional factors in the runoff processes need further investigation. These watersheds and their associated hydrological characteristics may have local-scale patterns that vary the peak flow generation. Wasko and

Sharma (2017) suggested that disagreement between extreme rainfall and streamflow may be attributed to antecedent soil moisture conditions for larger watersheds. In contrast, in our analysis, we found only small differences when considering antecedent rainfall (as indication of antecedent soil moisture conditions) and annual maximum peak flow. In our study, it was challenging to demonstrate how sensitive the PF_{max} is to antecedent soil moisture in Hawaiʻi by comparing with paired 1-day, 2-day, or 5-day accumulated rainfall. There are two possible reasons for this: 1) the PF_{max} is not sensitive to antecedent soil moisture likely due to the small watersheds with shorter concentration time in Hawaiʻi, or 2) the 5-day accumulated rainfall is insufficient to indicate the soil moisture maximum. The pairing methods adopted in this study have improved our understanding and representation of rainfall events that cause peak flows. However, it remains unclear why some of the pairs exhibit negative trend relationships, and thus further investigation is required. The change in RF_{max} cannot be conclusively applied as a proxy for the change in PF_{max}, and we must be cautious in predicting changes in extreme streamflow based on changes in extreme rainfall alone.

4.4 The shifts in seasonality of annual maximum rainfall and annual peak flow

The occurrence time of RF_{max} and PF_{max} has receded from late January to December in Hawaiʻi (Figure 5). In addition to the timing of winter storms, these temporal shifts in peak flow may be due to the soil moisture conditions. In continental or large watersheds (> 2000 km^2), changes in antecedent soil moisture play a notable part in temporal shifts of floods (Blöschl et al., 2017; Merz and Blöschl, 2003; Wasko and Sharma, 2017). Frazer and Gaimbelluca (2016) showed that Hawaiʻi had experienced drying trends from 1920-2012. However, it is unclear how drying conditions have impacted the timing of maximum soil moisture and the occurrence time of PF_{max}. Shifting climate patterns may also have altered atmospheric circulations and the timing of winter rainfall (Blöschl et al., 2017; Diaz et al., 2016, 2001), which would change the timing of RF_{max} and then PF_{max}. To our knowledge, no other studies have addressed temporal shifts of RF_{max} and PF_{max} in Hawaiʻi; hence this study provides an important contribution to our understanding of shifting hydrological regimes in Hawaiʻi. It also adds further information and raises the awareness of temporal shifts in both RF_{max} and PF_{max}.

The occurrence time of RF_{max} in both windward and leeward regions exhibited 2 to 7 years oscillations (Figures 5–7). These oscillations may be caused by ENSO or other large atmospheric cycles. Previous running trend analyses of the magnitude of monthly rainfall, extreme precipitation, and streamflow have also identified distinct associations with atmospheric oscillations (Chu et al., 2010; Clilverd et al., 2019; Frazier and Giambelluca, 2016). These oscillations are most likely due to natural coupled oceanic and atmospheric cycles, such as the ENSO. Chu et al. (2010) suggested that more extreme precipitation in the Hawaiian Islands occur during La Niña years, while fewer extreme precipitation events happen during El Niño years. However, we found no pronounced relationship between ENSO and the magnitude of RF_{max} and PF_{max}, with possible bias due to different methods and study periods. Instead, we discovered that the occurrence time of both RF_{max} and PF_{max} likely depends on the ENSO phase regardless of its strength. It is unsurprising that ENSO impacted the occurrence time of both RF_{max} and PF_{max}. Studies show that ENSO events delayed the starting time of monsoon in Asia (e.g., Joseph et al., 1994; Wang et al., 2013). Different El Niño properties might have led to different starting time of El Niño and thus on the timing of rainfall (Xin Wang et al., 2013; Bin Wang et al, 2019). Different mechanisms in occurrences of El Niño (e.g., the El Niño that had earlier starting time and occurred more frequent from 1901 to 2017 (Wang et al., 2019)) possibly contribute to the shift of occurrence time of RF_{max} and PF_{max}. The shifts in occurrence time have important ecological implications – for instance, the timing of flash floods triggers the migration of native freshwater fish, o‘opu, from their coastal nursery grounds to core stream habitats where they mature and reproduce (Fitzsimons and Nishimoto, 1995; Radtke and Kinzie, 1996). Therefore, shifts in the timing of these migratory cues could have consequences for the dispersal and life cycles of native stream species across the Hawaiian Islands. We need further research on the sensitivity of peak flow to natural climate oscillations and climate change, and the influence on the magnitude and seasonality of RF_{max} and PF_{max}. This could be addressed with new stream gauges in watersheds, a more extensive rainfall gauge network, and support for long-term records, that would provide more effective streams and rainfall pairs needed to further our understanding of the association between peak flow and rainfall. These would improve our understanding of the drivers of observed changes in seasonal peak flow and improve our ability to predict future flooding events across the Hawaiian Islands, and the potential impacts on humans and the ecosystem.

4.5 Conclusions

We have gained an improved understanding of local changes in peak streamflow and responses to changes in rainfall. Despite limitations in the availability of long-term data, our study demonstrated that both annual maximum rainfall and annual peak flow have declined; local responses of both extreme rainfall and streamflow were varied, and changes in peak streamflow do not necessarily follow the changes in maximum rainfall. In addition, we conclude that spatial linkages between rainfall and streamflow gauges are important when studying the relationship between peak streamflow and maximum rainfall. Also, the temporal shifts in peak streamflow and rainfall should be considered in understanding changes in extreme events. Examining the inconsistency between the timing of peak streamflow and annual maximum rainfall is much needed, and investigating the mechanisms that cause annual maximum rainfall or heavy rainfall could shed light on the subsequent results in temporal shifts in peak streamflow.

Acknowledgement

The authors acknowledge the support by the United States Department of Agriculture (USDA) National Institute of Food and Agriculture, McIntire Stennis project 1140M, and by National Science Foundation (NSF) Office of International and Integrative Activities (IIA), RII Track-4: Building the Next Generation Meteo-Hydrological Model for Hawaii (OIA-1929155).

References

Alexander, L. V., Zhang, X., Peterson, T.C., Caesar, J., Gleason, B., Klein Tank, A.M.G., Haylock, M., Collins, D., Trewin, B., Rahimzadeh, F., Tagipour, A., Rupa Kumar, K., Revadekar, J., Griffiths, G., Vincent, L., Stephenson, D.B., Burn, J., Aguilar, E., Brunet, M., Taylor, M., New, M., Zhai, P., Rusticucci, M., Vazquez-Aguirre, J.L., 2006. Global observed changes in daily climate extremes of temperature and precipitation. J. Geophys. Res. Atmos. 111, 1–22. https://doi.org/10.1029/2005JD006290

Bassiouni, M., Oki, D.S., 2013. Trends and shifts in streamflow in Hawai'i, 1913-2008. Hydrol. Process. 27, 1484–1500. https://doi.org/10.1002/hyp.9298

Beck, F., Bárdossy, A., Seidel, J., Müller, T., Fernandez Sanchis, E., Hauser, A., 2015. Statistical analysis of sub-daily precipitation extremes in Singapore. J. Hydrol. Reg. Stud. 3, 337–358. https://doi.org/10.1016/j.ejrh.2015.02.001

Blöschl, G., Hall, J., Parajka, J., Perdigão, R.A.P., Merz, B., Arheimer, B., Aronica, G.T., Bilibashi, A., Bonacci, O., Borga, M., Čanjevac, I., Castellarin, A., Chirico, G.B., Claps, P., Fiala, K., Frolova, N., Gorbachova, L., Gül, A., Hannaford, J., Harrigan, S., Kireeva, M., Kiss, A., Kjeldsen, T.R., Kohnová, S., Koskela, J.J., Ledvinka, O., Macdonald, N., Mavrova-Guirguinova, M., Mediero, L., Merz, R., Molnar, P., Montanari, A., Murphy, C., Osuch, M., Ovcharuk, V., Radevski, I., Rogger, M., Salinas, J.L., Sauquet, E., Šraj, M., Szolgay, J., Viglione, A., Volpi, E., Wilson, D., Zaimi, K., Živković, N., 2017. Changing climate shifts timing of European floods. Science 357, 588–590. https://doi.org/10.1126/science.aan2506

Blöschl, G., Hall, J., Viglione, A., Perdigão, R.A.P., Parajka, J., Merz, B., Lun, D., Arheimer, B., Aronica, G.T., Bilibashi, A., Boháč, M., Bonacci, O., Borga, M., Čanjevac, I., Castellarin, A., Chirico, G.B., Claps, P., Frolova, N., Ganora, D., Gorbachova, L., Gül, A., Hannaford, J., Harrigan, S., Kireeva, M., Kiss, A., Kjeldsen, T.R., Kohnová, S., Koskela, J.J., Ledvinka, O., Macdonald, N., Mavrova-Guirguinova, M., Mediero, L., Merz, R., Molnar, P., Montanari, A., Murphy, C., Osuch, M., Ovcharuk, V., Radevski, I., Salinas, J.L., Sauquet, E., Šraj, M., Szolgay, J., Volpi, E., Wilson, D., Zaimi, K., Živković, N., 2019. Changing climate both increases and decreases European river floods. Nature 573, 108–111. https://doi.org/10.1038/s41586-019-1495-6

Cao, G., Giambelluca, T.W., Stevens, D.E., Schroeder, T.A., 2007. Inversion Variability in the Hawaiian Trade Wind Regime. J. Clim. 20, 1145–1160. https://doi.org/10.1175/JCLI4033.1

Caruso, S.J., Businger, S., 2006. Subtropical cyclogenesis over the central North Pacific. Weather Forecast. 21, 193–205. https://doi.org/10.1175/WAF914.1

Changnon, B.S.A., Kunkep, K.E., 1995. Climate-related fluctuations in midwestern floods during 1921-1985 121, 326–334.

Chen, Y.R., Chu, P.S., 2014. Trends in precipitation extremes and return levels in the Hawaiian Islands under a changing climate. Int. J. Climatol. 34, 3913–3925. https://doi.org/10.1002/joc.3950

Chu, P.-S., Nash, A.J., Porter, F.-Y., 1993. Diagnostic studies of two contrasting rainfall episodes in Hawaii: dry 1981 and wet 1982. J. Clim. 6, 1457–1462.

Chu, P.-S., Wang, J., 1997. Tropical cyclone occurrences in the vicinity of Hawaii: Are the differences between El Niño and non--El Niño years significant? J. Clim. 10, 2683–2689.

Chu, P.S., Chen, H., 2005. Interannual and interdecadal rainfall variations in the Hawaiian Islands. J. Clim. 18, 4796–4813. https://doi.org/10.1175/JCLI3578.1

Chu, P.S., Chen, Y.R., Schroeder, T.A., 2010. Changes in precipitation extremes in the Hawaiian

Islands in a warming climate. J. Clim. 23, 4881–4900. https://doi.org/10.1175/2010JCLI3484.1

Clilverd, H.M., Tsang, Y.-P., Infante, D.M., Lynch, A.J., Strauch, A.M., 2019. Long-term streamflow trends in Hawaiʻi and implications for native stream fauna. Hydrol. Process. 33, 699–719. https://doi.org/10.1002/hyp.13356

Climate Prediction Center (CPC), 2019. El Niño-Southern Oscillation (ENSO) Oceanic Niño Index (ONI) from ERSSTv5) [WWW Document]. URL https://origin.cpc.ncep.noaa.gov/products/analysis_monitoring/ensostuff/ONI_v5.php (accessed 9.22.20).

Craig, D.A., 2003. Geomorphology, development of running water habitats, and evolution of black flies on Polynesian Islands. Bioscience 53, 1079–1093. https://doi.org/10.1641/0006-3568(2003)053[1079:GDORWH]2.0.CO;2

Cunderlik, J.M., Ouarda, T.B.M.J., 2009. Trends in the timing and magnitude of floods in Canada. J. Hydrol. 375, 471–480. https://doi.org/10.1016/j.jhydrol.2009.06.050

Diaz, H.F., Giambelluca, T.W., 2012. Changes in atmospheric circulation patterns associated with high and low rainfall regimes in the Hawaiian Islands region on multiple time scales. Glob. Planet. Change 98–99, 97–108. https://doi.org/10.1016/j.gloplacha.2012.08.011

Diaz, H.F., Hoerling, M.P., Eischeid, J.K., 2001. ENSO variability, teleconnections and climate change. Int. J. Climatol. 21, 1845–1862. https://doi.org/10.1002/joc.631

Diaz, H.F., Wahl, E.R., Zorita, E., Giambelluca, T.W., Eischeid, J.K., 2016. A five-century reconstruction of Hawaiian Islands winter rainfall. J. Clim. 29, 5661–5674. https://doi.org/10.1175/JCLI-D-15-0815.1

Do, H.X., Westra, S., Leonard, M., 2017. A global-scale investigation of trends in annual maximum streamflow. J. Hydrol. 552, 28–43. https://doi.org/10.1016/j.jhydrol.2017.06.015

Donat, M.G., Alexander, L. V., Yang, H., Durre, I., Vose, R., Dunn, R.J.H., Willett, K.M., Aguilar, E., Brunet, M., Caesar, J., Hewitson, B., Jack, C., Klein Tank, A.M.G., Kruger, A.C., Marengo, J., Peterson, T.C., Renom, M., Oria Rojas, C., Rusticucci, M., Salinger, J., Elrayah, A.S., Sekele, S.S., Srivastava, A.K., Trewin, B., Villarroel, C., Vincent, L.A., Zhai, P., Zhang, X., Kitching, S., 2013. Updated analyses of temperature and precipitation extreme indices since the beginning of the twentieth century: The HadEX2 dataset. J. Geophys. Res. Atmos. 118, 2098–2118. https://doi.org/10.1002/jgrd.50150

Douglas, E.M., Vogel, R.M., Kroll, C.N., 2000. Trends in floods and low flows in the United States: Impact of spatial correlation. J. Hydrol. 240, 90–105. https://doi.org/10.1016/S0022-1694(00)00336-X

Easterling, D.R., Kunkel, K.E., Arnold, J.R., Knutson, T.R., LeGrande, A.N., Leung, L.R., Vose, R.S., Waliser, D.E., Wehner, M., 2017. Precipitation change in the United States. Clim. Sci. Spec. Rep. Fourth Natl. Clim. Assessment, Vol. I I, 207–230. https://doi.org/10.7930/J0H993CC.U.S.

Elison Timm, O., Diaz, H.F., Giambelluca, T.W., Takahashi, M., 2011. Projection of changes in the frequency of heavy rain events over Hawaii based on leading Pacific climate modes. J. Geophys. Res. Atmos. 116, 1–12. https://doi.org/10.1029/2010JD014923

Fitzsimons, J.M., Nishimoto, R.T., 1995. Use of fish behavior in assessing the effects of Hurricane Iniki on the Hawaiian island of Kaua'i. Environ. Biol. Fishes 43, 39–50. https://doi.org/10.1007/BF00001816

Frazier, A.G., Deenik, J.L., Fujii, N.D., Funderburk, G.R., Giambelluca, T.W., Giardina, C.P., Helweg, D.A., Keener, V.W., Mair, A., Marra, John J, Mcdaniel, S., Ohye, L.N., Oki, D.S., Parsons, E.W., Strauch, A.M., Trauernicht, C., Marra, J J, 2019. Drought in Hawai'i and U.S. affiliated Pacific Islands, general technical report: Effects of drought on range lands and forests in the United States.

Frazier, A.G., Giambelluca, T.W., 2016. Spatial trend analysis of Hawaiian rainfall from 1920 to 2012. Int. J. Climatol. https://doi.org/10.1002/joc.4862

Frazier, A.G.A.G., Elison Timm, O., Giambelluca, T.W.T.W., Diaz, H.F.H.F., 2017. The influence of ENSO, PDO and PNA on secular rainfall variations in Hawaiʻi. Clim. Dyn. 0, 0. https://doi.org/10.1007/s00382-017-4003-4

Giambelluca, T.W., Chen, Q., Frazier, A.G., Price, J.P., Chen, Y.-L., Chu, P.-S., Eischeid, J.K., Delparte, D.M., 2013. Online rainfall atlas of Hawaiʻi. Bull. Am. Meteorol. Soc. 94, 313–316. https://doi.org/10.1175/BAMS-D-11-00228.1

Groisman, P.Y., Knight, R.W., Easterling, D.R., Karl, T.R., Hegerl, G.C., Razuvaev, V.N., 2005. Trends in intense precipitation in the climate record. J. Clim. 18, 1326–1350. https://doi.org/10.1175/JCLI3339.1

Groisman, P.Y., Knight, R.W., Karl, T.R., 2001. Heavy precipitation and high streamflow in the contiguous United States: trends in the twentieth century. Bull. Am. Meteorol. Soc. 82, 219–246. https://doi.org/10.1175/1520-0477(2001)082<0219:HPAHSI>2.3.CO;2

Groisman, P.Y., Knight, R.W., Karl, T.R., Easterling, D.R., Sun, B., Lawrimore, J.H., 2004. Contemporary changes of the hydrological cycle over the contiguous United States: trends derived from in situ observations. J. Hydrometeorol. 5, 64–85. https://doi.org/10.1175/1525-7541(2004)005<0064:CCOTHC>2.0.CO;2

Hannaford, J., Marsh, T.J., 2008. High-flow and flood trends in a network of undisturbed catchments in the UK. Int. J. Climatol. 28, 1325–1338. https://doi.org/10.1002/joc.1643

Held, I.M., Soden, B.J., Held, I.M., Soden, B.J., 2006. Robust Responses of the Hydrological Cycle to Global Warming. J. Clim. 19, 5686–5699. https://doi.org/10.1175/JCLI3990.1

Hirsch, R.M., Slack, J.R., 1984. A nonparametric trend test for seasonal data with serial dependence. Water Resour. Res. 20, 727–732. https://doi.org/10.1029/WR020i006p00727

Ishak, E.H., Rahman, A., Westra, S., Sharma, A., Kuczera, G., 2013. Evaluating the non-stationarity of australian annual maximum flood. J. Hydrol. 494, 134–145. https://doi.org/10.1016/j.jhydrol.2013.04.021

Ivancic, T.J., Shaw, S.B., 2015. Examining why trends in very heavy precipitation should not be mistaken for trends in very high river discharge. Clim. Change 133, 681–693. https://doi.org/10.1007/s10584-015-1476-1

Jin, F.-F., Boucharel, J., Lin, I.-I., 2014. Eastern Pacific tropical cyclones intensified by El Niño delivery of subsurface ocean heat. Nature 516, 82–85. https://doi.org/10.1038/nature13958

Joseph, P. V., Eischeid, J.K., Pyle, R.J., 1994. Interannual Variability of the Onset of the Indian Summer Monsoon and Its Association with Atmospheric Features, El Niño, and Sea Surface Temperature Anomalies. J. Clim. 7, 81–105. https://doi.org/10.1175/1520-0442(1994)007<0081:IVOTOO>2.0.CO;2

Klotzbach, P.J., 2006. Trends in global tropical cyclone activity over the past twenty years (1986-2005). Geophys. Res. Lett. 33, 1984–1987. https://doi.org/10.1029/2006GL025881

Kodama, K., Barnes, G.M., 1997. Heavy rain events over the south-facing slopes of Hawaii: Attendant conditions. Weather Forecast. 12, 347–367. https://doi.org/10.1175/1520-0434(1997)012<0347:HREOTS>2.0.CO;2

Knutson, T.R., Manabe, S., 1995. Time-mean response over the tropical Pacific to increased CO2 in a coupled ocean-atmosphere model. J. Clim. 8, 2181–2199.

Li, T., Kwon, M., Zhao, M., Kug, J.S., Luo, J.J., Yu, W., 2010. Global warming shifts Pacific tropical cyclone location. Geophys. Res. Lett. 37, 1–5. https://doi.org/10.1029/2010GL045124

Lins, H.F., Slack, J.R., 1999. Streamflow trends in the United States. Geophys. Res. Lett. 26, 227–230. https://doi.org/10.1029/1998GL900291

Lund, U., Agostinelli, C., Agostinelli, M.C., 2017. Package ‘circular.’ Repos. CRAN.

Luo, X., Wang, B., Frazier, A.G., Giambelluca, T.W., 2020. Distinguishing Variability Regimes of Hawaiian Summer Rainfall: Quasi-Biennial and Interdecadal Oscillations. Geophys. Res. Lett. 47. https://doi.org/10.1029/2020GL091260

Lyons, S.W., 1982. Empirical orthogonal function analysis of Hawaiian rainfall. J. Appl. Meteorol. 21, 1713–1729. https://doi.org/10.1175/1520-0450(1982)021<1713:EOFAOH>2.0.CO;2

Madsen, H., Lawrence, D., Lang, M., Martinkova, M., Kjeldsen, T.R., 2014. Review of trend analysis and climate change projections of extreme precipitation and floods in Europe. J. Hydrol. 519, 3634–3650. https://doi.org/10.1016/j.jhydrol.2014.11.003

Mann, H.B., 1945. Nonparametric tests against trend. Econometrica 13, 245. https://doi.org/10.2307/1907187

Mantua, N.J., Hare, S.R., Zhang, Y., Wallace, J.M., Francis, R.C., 1997. A Pacific interdecadal climate oscillation with impacts on salmon production. Bull. Am. Meteorol. Soc. 78, 1069–1079. https://doi.org/10.1175/1520-0477(1997)078<1069:APICOW>2.0.CO;2

Mediero, L., Santillán, D., Garrote, L., Granados, A., 2014. Detection and attribution of trends in magnitude, frequency and timing of floods in Spain. J. Hydrol. 517, 1072–1088.

Merz, R., Blöschl, G., 2003. A process typology of regional floods. Water Resour. Res. 39.

https://doi.org/10.1029/2002WR001952

Murakami, H., Wang, B., Li, T., Kitoh, A., 2013. Projected increase in tropical cyclones near Hawaii. Nat. Clim. Chang. 3, 749–754. https://doi.org/10.1038/nclimate1890

National Centers for Environmental Information (NCEI), 2019a. Storm events database [WWW Document]. URL https://www.ncdc.noaa.gov/stormevents/ (accessed 9.22.20).

National Centers for Environmental Information (NCEI), 2019b. Pacific decadal oscillation (PDO) [WWW Document]. URL https://www.ncdc.noaa.gov/teleconnections/pdo/ (accessed 9.22.20).

Nugent, A.D., Longman, R.J., Trauernicht, C., Lucas, M.P., Diaz, H.F., Giambelluca, T.W., 2020. Fire and Rain: The Legacy of Hurricane Lane in Hawai'i. Bull. Am. Meteorol. Soc. 101, E954–E967. https://doi.org/10.1175/BAMS-D-19-0104.1O'Connor, C.F., Chu, P.-S., Hsu, P.-C., Kodama, K., 2015. Variability of Hawaiian Winter Rainfall during La Niña Events since 1956. J. Clim. 28, 7809–7823. https://doi.org/10.1175/JCLI-D-14-00638.1

Oki, D.S., 2004. Trends in streamflow characteristics in Hawaii, 1913-2002. U.S. Geol. Surv. Fact Sheet 2004-3104 4 p.

Oki, D.S., 2003. Surface water in Hawaii. U.S. Geol. Surv. Fact Sheet 045-03 6 p. (2–sided 3–part fold).

Petrow, T., Merz, B., 2009. Trends in flood magnitude, frequency and seasonality in Germany in the period 1951-2002. J. Hydrol. 371, 129–141. https://doi.org/10.1016/j.jhydrol.2009.03.024

Pewsey, A., Neuhäuser, M., Ruxton, G.D., 2013. Circular statistics in R. Oxford University Press.

Pingale, S.M., Khare, D., Jat, M.K., Adamowski, J., 2014. Spatial and temporal trends of mean and extreme rainfall and temperature for the 33 urban centers of the arid and semi-arid state of Rajasthan, India. Atmos. Res. 138, 73–90. https://doi.org/10.1016/j.atmosres.2013.10.024

Pohlert, T., Pohlert, M.T., Test, M.-K.T., Test, B.U., Test, S.N.H., 2018. Package ‘trend.’

Radtke, R.L., Kinzie, R.A., 1996. Evidence of a marine larval stage in endemic Hawaiian stream gobies from isolated high-elevation locations. Trans. Am. Fish. Soc. 125, 613–621. https://doi.org/10.1577/1548-8659(1996)125<0613:EOAMLS>2.3.CO;2

Renard, B., Lang, M., Bois, P., Dupeyrat, A., Mestre, O., Niel, H., Sauquet, E., Prudhomme, C., Parey, S., Paquet, E., Neppel, L., Gailhard, J., 2008. Regional methods for trend detection: Assessing field significance and regional consistency. Water Resour. Res. 44. https://doi.org/10.1029/2007WR006268

Sahoo, G.B., Ray, C., De Carlo, E.H., 2006. Use of neural network to predict flash flood and attendant water qualities of a mountainous stream on Oahu, Hawaii. J. Hydrol. 327, 525–538. https://doi.org/10.1016/j.jhydrol.2005.11.059

Sen, P.K., 1968. Estimates of the regression coefficient based on Kendall’s Tau. J. Am. Stat. Assoc. 63, 1379–1389. https://doi.org/10.1080/01621459.1968.10480934

Small, D., Islam, S., Vogel, R.M., 2006. Trends in precipitation and streamflow in the eastern U.S.: Paradox or perception? Geophys. Res. Lett. 33, 2–5. https://doi.org/10.1029/2005GL024995

Trenberth, K., 2011. Changes in precipitation with climate change. Clim. Res. 47, 123–138. https://doi.org/10.3354/cr00953

Trenberth, K.E., Hoar, T.J., 1997. El Niño and climate change. Geophys. Res. Lett. 24, 3057–3060. https://doi.org/10.1029/97GL03092

Wang, B., Luo, X., Yang, Y.M., Sun, W., Cane, M.A., Cai, W., Yeh, S.W., Liu, J., 2019. Historical change of El Niño properties sheds light on future changes of extreme El Niño. Proc. Natl. Acad. Sci. U. S. A. 116, 22512–22517. https://doi.org/10.1073/pnas.1911130116

Wang, X., Jiang, X., Yang, S., Li, Y., 2013. Different impacts of the two types of El Niño on Asian summer monsoon onset. Environ. Res. Lett. 8. https://doi.org/10.1088/1748-9326/8/4/044053

Wasko, C., Sharma, A., 2017. Global assessment of flood and storm extremes with increased temperatures. Sci. Rep. 7, 1–8. https://doi.org/10.1038/s41598-017-08481-1

Wentz, F.J., Ricciardulli, L., Hilburn, K., Mears, C., 2007. How much more rain will global warming bring? Science 317, 233–235. https://doi.org/10.1126/science.1140746

Westra, S., Alexander, L. V., Zwiers, F.W., 2013. Global increasing trends in annual maximum daily precipitation. J. Clim. 26, 3904–3918. https://doi.org/10.1175/JCLI-D-12-00502.1

Zar, J.H., 1999. Biostatistical analysis. Pearson Education India.

Zhang, X.S., Amirthanathan, G.E., Bari, M.A., Laugesen, R.M., Shin, D., Kent, D.M., MacDonald, A.M., Turner, M.E., Tuteja, N.K., 2016. How streamflow has changed across Australia since the 1950s: evidence from the network of hydrologic reference stations. Hydrol. Earth Syst. Sci. 20, 3947–3965. https://doi.org/10.5194/hess-20-3947-2016

Table 1 Trends of annual peak flow and trends of 1-day, 2-day, and 5-day accumulated rainfall of the same date as the annual peak flow for each pair (see figure 4 for the spatial distribution) between 1970 and 2005. Trends are shown in percent change per year, and the consistent trends (with the same sign) between peak flow and paired rainfall are shaded in grey. (OA = O‘ahu, KA = Kaua‘i, MO = Moloka‘i, MA = Maui, HA = Hawai‘i, and ‘*’: p-value < 0.05, ‘**’: p-value < 0.01, ‘***’: p-value < 0.00)

Island	Rain Gauge	Crest gauge	peak flow (%)	1-day rainfall (%)	2-day rainfall (%)	5-day rainfall (%)
KA	USC00515560	16060000	0.38	-4.48*	-5.87	27.01
KA	USC00514561	16097900	-0.3	-1.41	-4.21	-1.8
OA	X213215157552800	16200000	0	-1.73	-1.17	-1.17
OA	X213215157552800	16208000	-0.43	-2.55	-2.45	-2.45
OA	X213215157552800	16212700	1.28	-0.94	-1.12	-1.12
OA	USC00518964	16212800	0.6	1.29	1.14	1.14
OA	USC00517810	16232000	0.57	0.04	-0.23	-0.23
OA	USC00517810	16237500	-1.48	-1.66	-2.56	-2.56
OA	USC00517810	16238500	2.45	1.03	0.34	0.34
OA	USC00517810	16240500	0.12	0.15	-0.07	-0.07
OA	USC00517664	16244000	5.77*	2.57	1.79	1.79
OA	USC00517664	16247100	0.26	0.11	-0.34	-0.34
OA	USC00519523	16249000	-0.6	-0.57	-1.13	-1.13
OA	USC00513117	16274499	-0.91	-3.2	-3.07	-3.07
OA	USC00518964	16294900	-0.77	0.63	4.84	4.84
OA	X213215157552800	16296500	0.77	-1.65	-1.17	-1.17
OA	X213215157552800	16301050	0.67	-0.13	0	0
MO	USW00022534	16411800	-6.54	18.74	19.13	13.55
MA	USC00511125	16502400	0.4	0.22	0.62	-0.36
MA	USC00511125	16502800	1.41	-0.55	-0.5	0.08
MA	USC00511125	16502900	1.25	1.05	1.23	1
MA	USC00511004	16587000	0.59	-1.07	-0.44	-1.73
MA	USC00511004	16603700	-4.58*	-1.13	-0.69	-1.22
MA	USC00511004	16603800	-1.59	-1.54	-1.94	-1.69

MA	USC00518543	16603850	2.41	2.41	2.9	-2.36
MA	USC00515715	16630200	-0.21	-5.49*	-8.23	-11.49
MA	USC00515177	16638500	1.75	-2.67	-0.83	0
MA	USC00515408	16643300	-0.13	-3.78	-5.19	-4.89
MA	USC00517059	16646200	-0.28	-3.66	-2.24	-1.92
MA	USC00518060	16647500	-0.04	-0.56	-1.49	-0.55
MA	USC00511004	16658500	2.69	2.34	2.15	-3.11
MA	USC00514489	16659000	-0.85	6.02	8.83	7.88
HA	USC00519025	16701300	1.61	-0.83	1.18	-2.1
HA	USC00519025	16701400	-8.15	-6.45	-1.86	-8.75
HA	USC00511065	16704000	-1.08	-3.81	-0.22	0.63
HA	USC00519025	16717000	-0.46	1.51	1.45	1.06
HA	USC00517312	16717850	-33.11	-24.6	-9.9	-5.39
HA	USC00514680	16752600	9.16	1.26	11.95	17.78
HA	USC00513300	16770500	0.99	-3.74	3.54	2.03

Figures

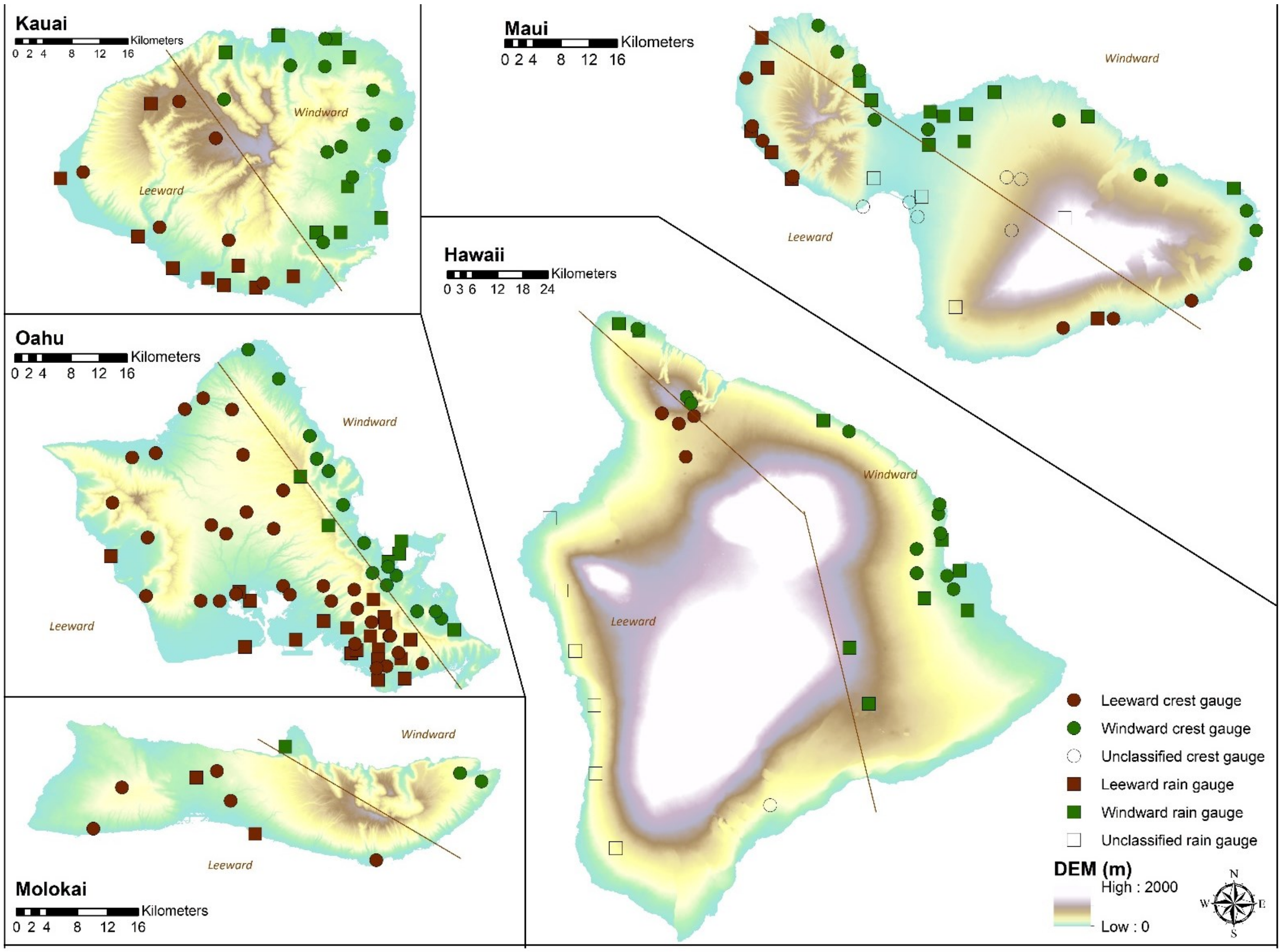

Figure 1 Map of crest (circles) and rain (squares) gauges in different physiographic zones – windward (green), leeward (brown), and unclassified (transparent) superimposed on the digital elevation model (DEM) obtained from the U.S. Geological Survey across five major Hawaiian Islands; the brown line indicates the physiographic division of windward (northeast) and leeward (southwest) regions on the islands.

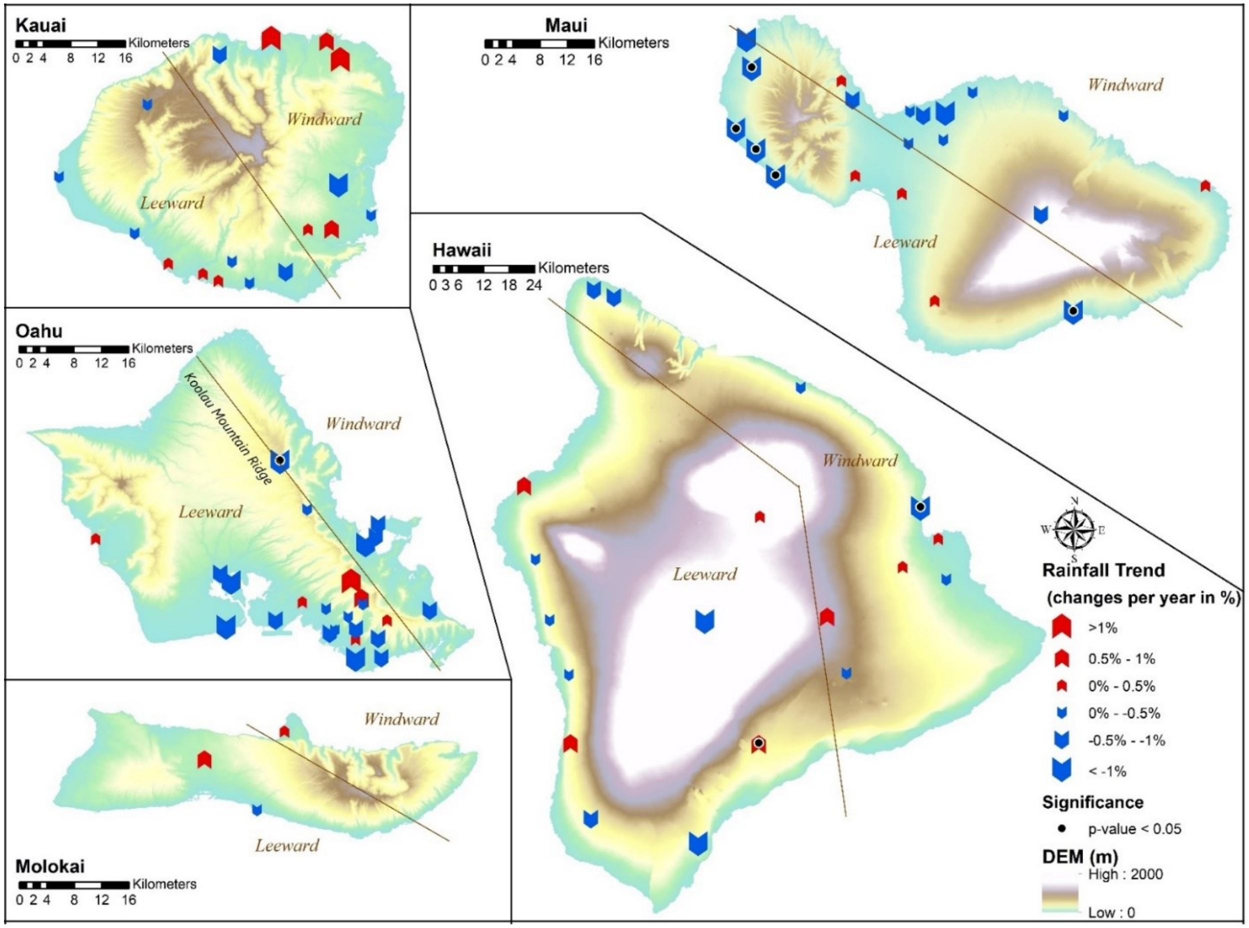

Figure 2 Annual maximum daily rainfall trends from water years 1970 to 2005 across five major Hawaiian Islands, superimposed on the DEM obtained from the U.S. Geological Survey. Blue inverted arrows show decreasing trends, red arrows show increasing trends, and black dots indicate significant trends ($p < 0.05$). The trends denote percentage change per year. The brown line indicates the physiographic division of windward (northeast) and leeward (southwest) regions on the islands.

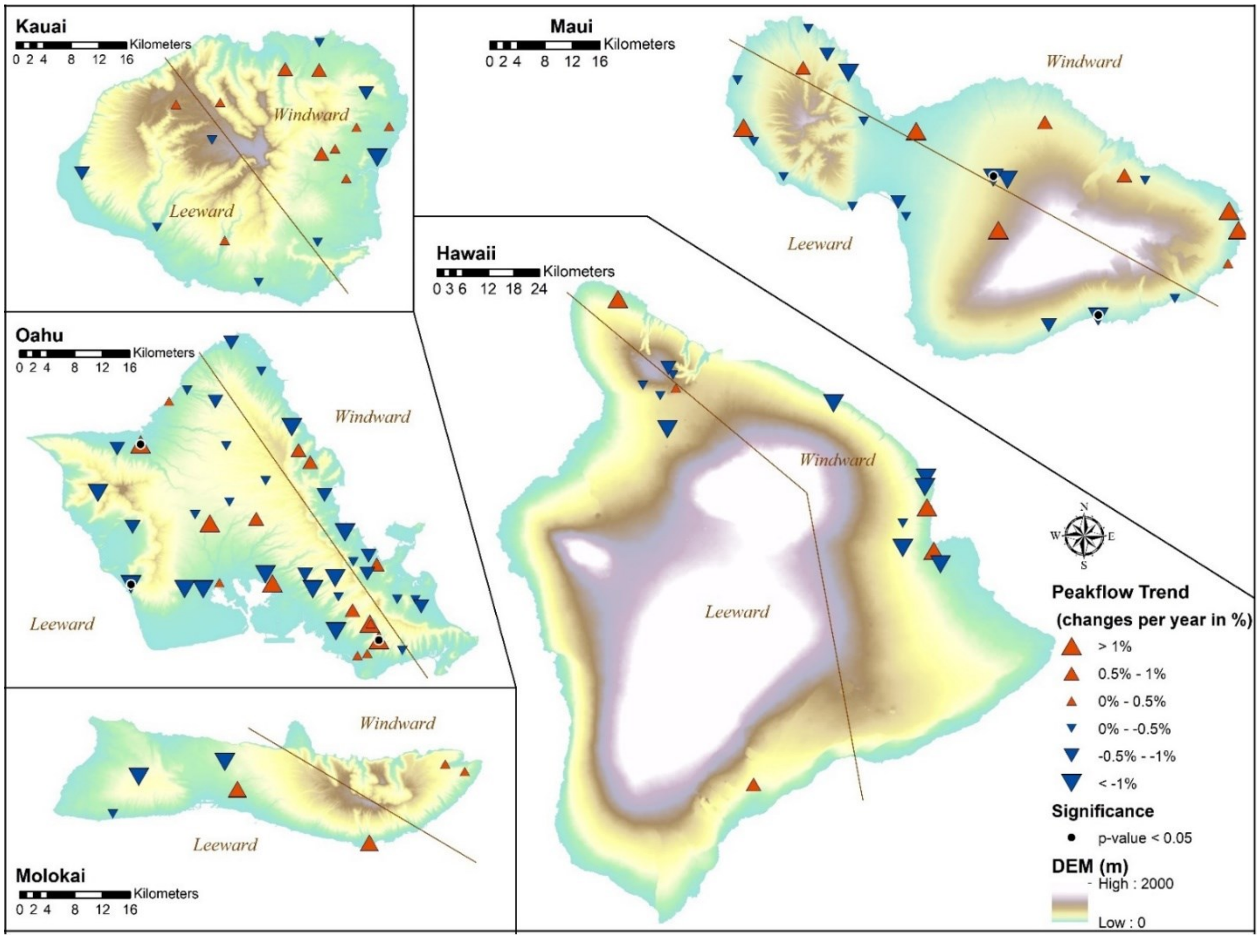

Figure 3 Annual peak flow trends from the water year 1970 to 2005 for the five main Hawaiian Islands. Blue inverted triangles show decreasing trends, the orange triangles show increasing trends, triangles with a black dot indicate significance ($p < 0.05$). The trends indicate percentage change per year. The color shading is the elevation (m). The brown line indicates the physiographic division of windward (northeast) and leeward (southwest) regions on the islands.

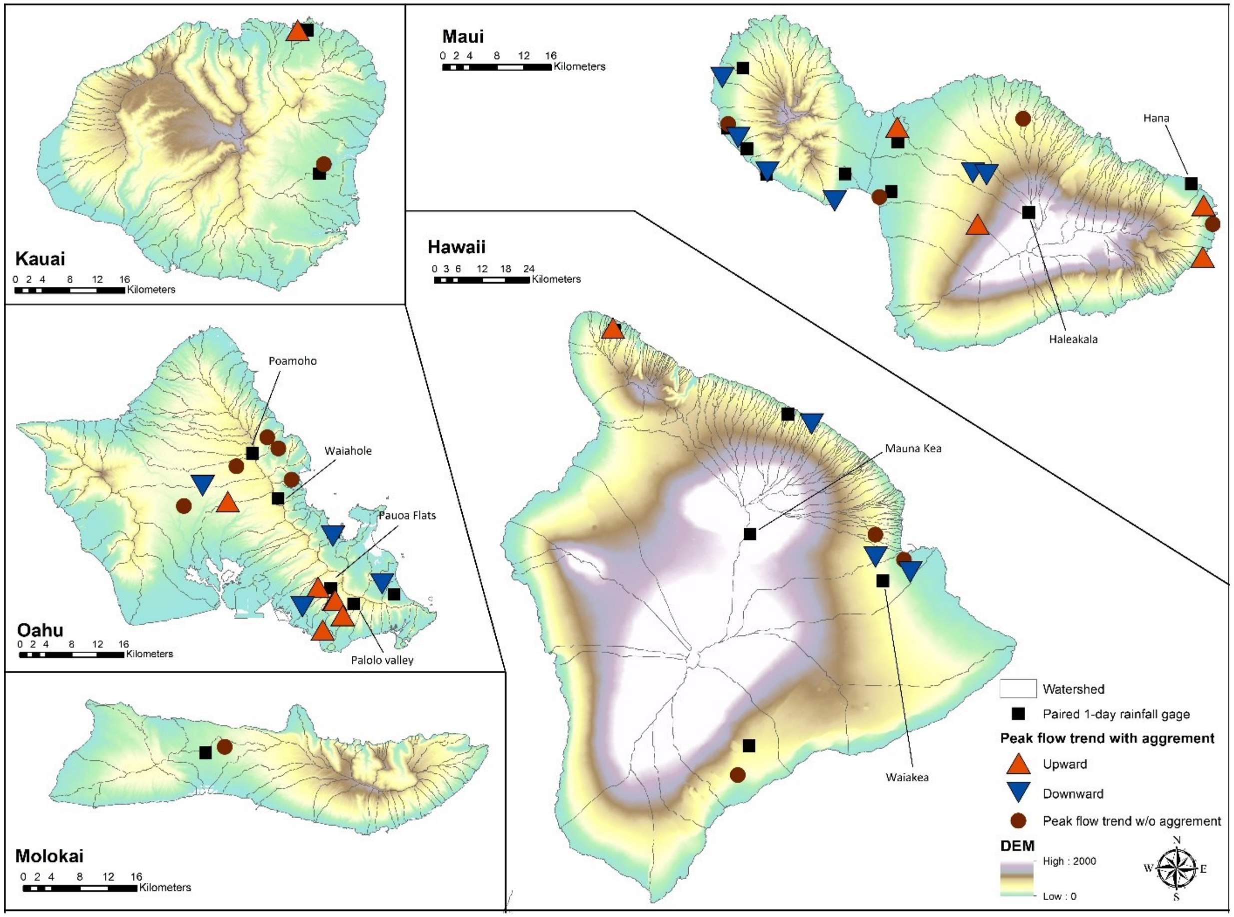

Figure 4 Paired daily rainfall and annual peak flow trends that showed agreement in the direction of trends from 1970 to 2005 for five major Hawaiian Islands, superimposed on the DEM obtained from the U.S. Geological Survey. Brown lines indicate the watershed boundaries. The paired daily rainfall gauge (black square) and the crest gauge (triangles) exhibit the same trend (peak flow trend with agreement; blue triangle: decreasing peak flow trends and can be referred to paired daily rainfall; orange triangle: increasing trends of peak flow and can be referred to paired daily rainfall). Brown circles show the crest gauges that did not have consistent trends with the paired rainfall (peak flow trend w/o agreement).

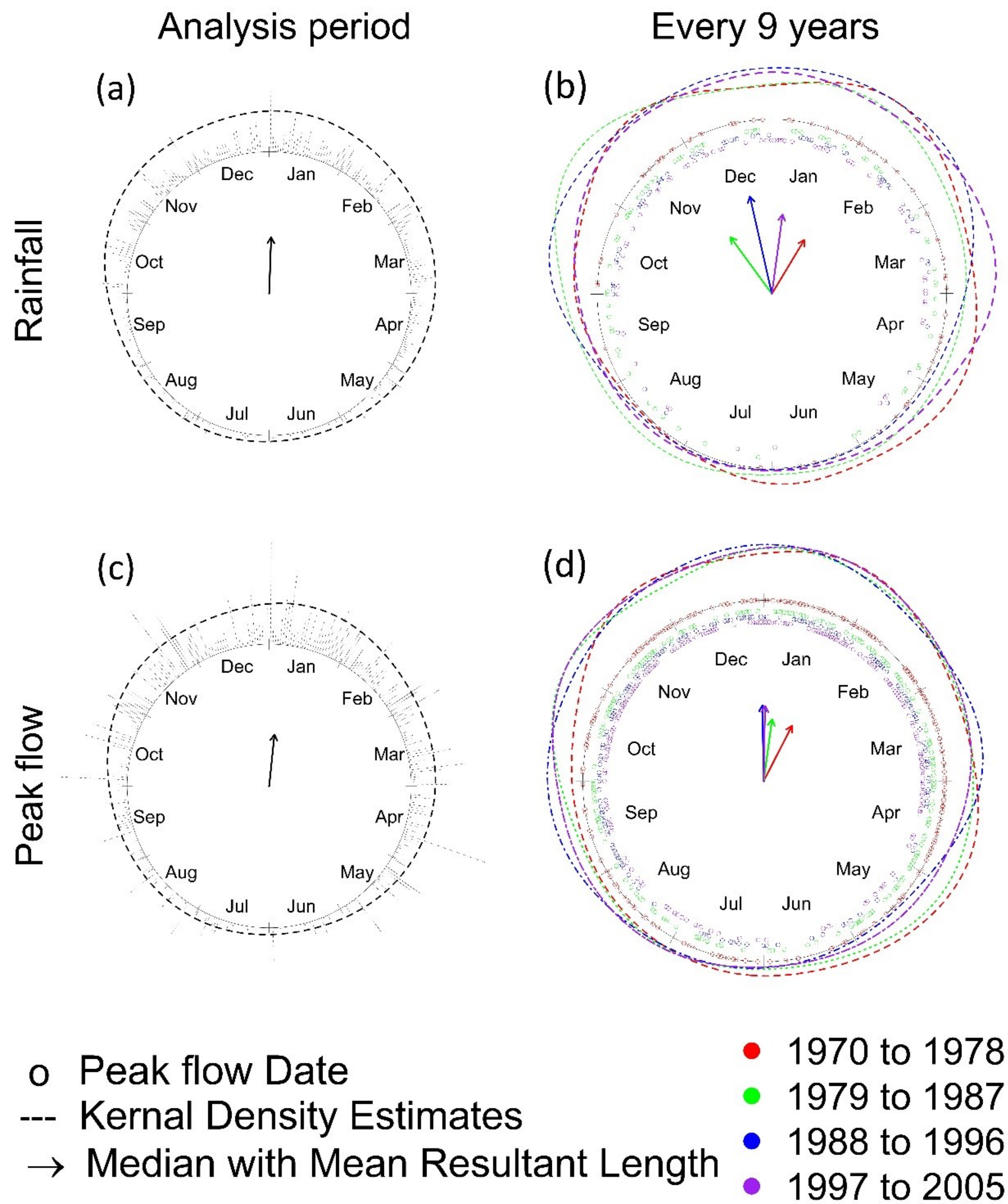

Figure 5 Comparison of the occurrence time of annual maximum daily rainfall (n=85 gauges) for (a) the analysis period, 1970-2005, and (c) every nine years from 1970-2005, with the occurrence time of annual peak flow (n=112 gauges) for (b) the analysis period, 1970-2005, and (d) for every nine years from 1910-2005, across the Hawaiian Islands. The dashed line is the estimated kernel density, and the arrow points to the median date of occurrence with mean resultant length. For (a) and (b), the gray dots indicate the frequency of the occurrence time. For (c) and (d), the colors reflect the time period, and the circles around the clock indicate the occurrence time.

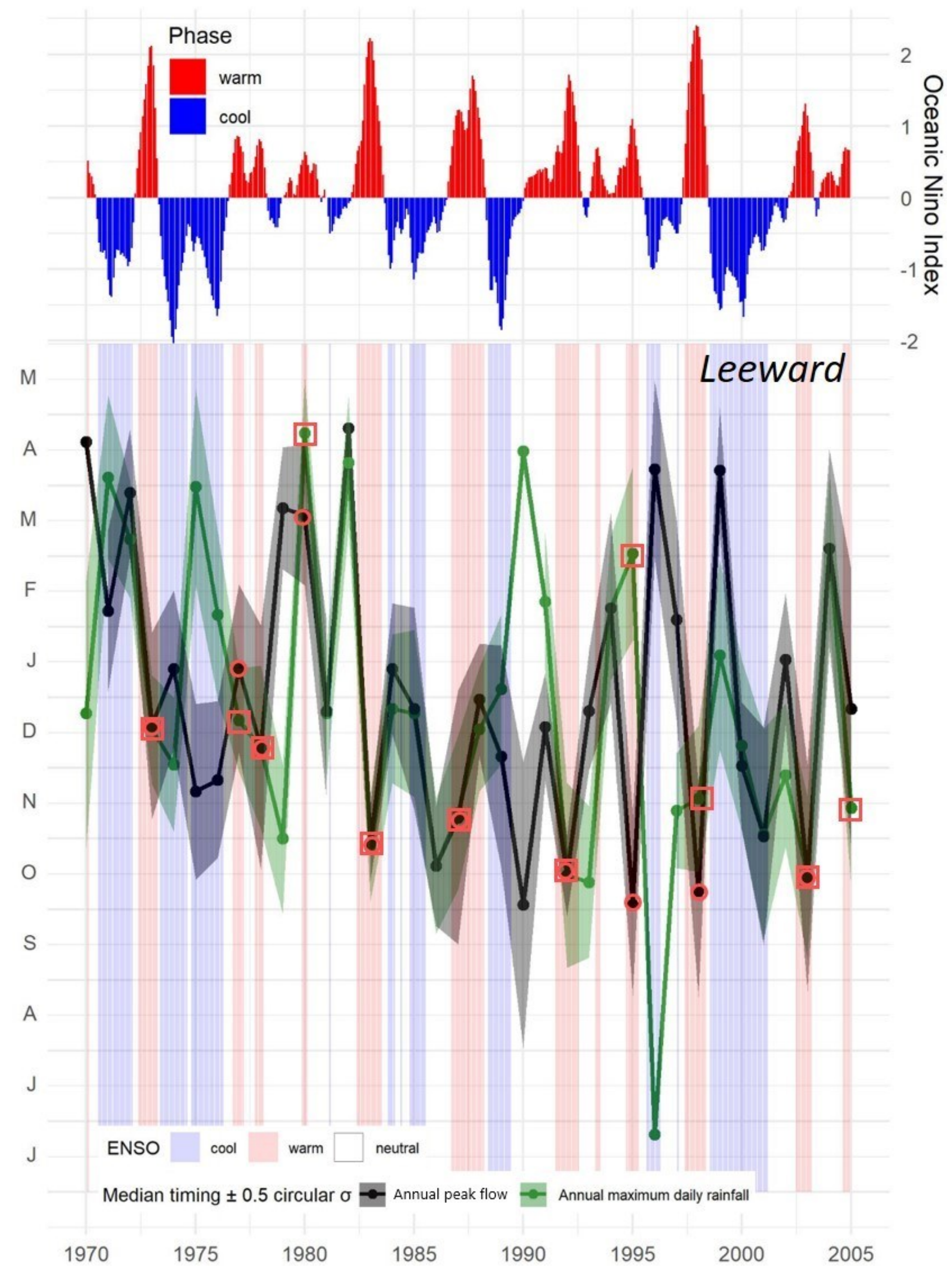

Figure 6 The occurrence time (median ± 0.5 circular deviation) of annual maximum daily rainfall (green line; n=42) and annual peak flow (black line; n=54) on the leeward side with the ENSO phase shaded (red: warm phase; blue: cool phase, white: neutral). The y-axis indicates the months from June through May (bottom to top). Occurrences under ENSO warm phase are indicated by red squares for annual maximum daily rainfall, and a red circle for annual peak flow. The Oceanic Nino Index (ONI) on the top indicates the strength of the ENSO from 1970 to 2005.

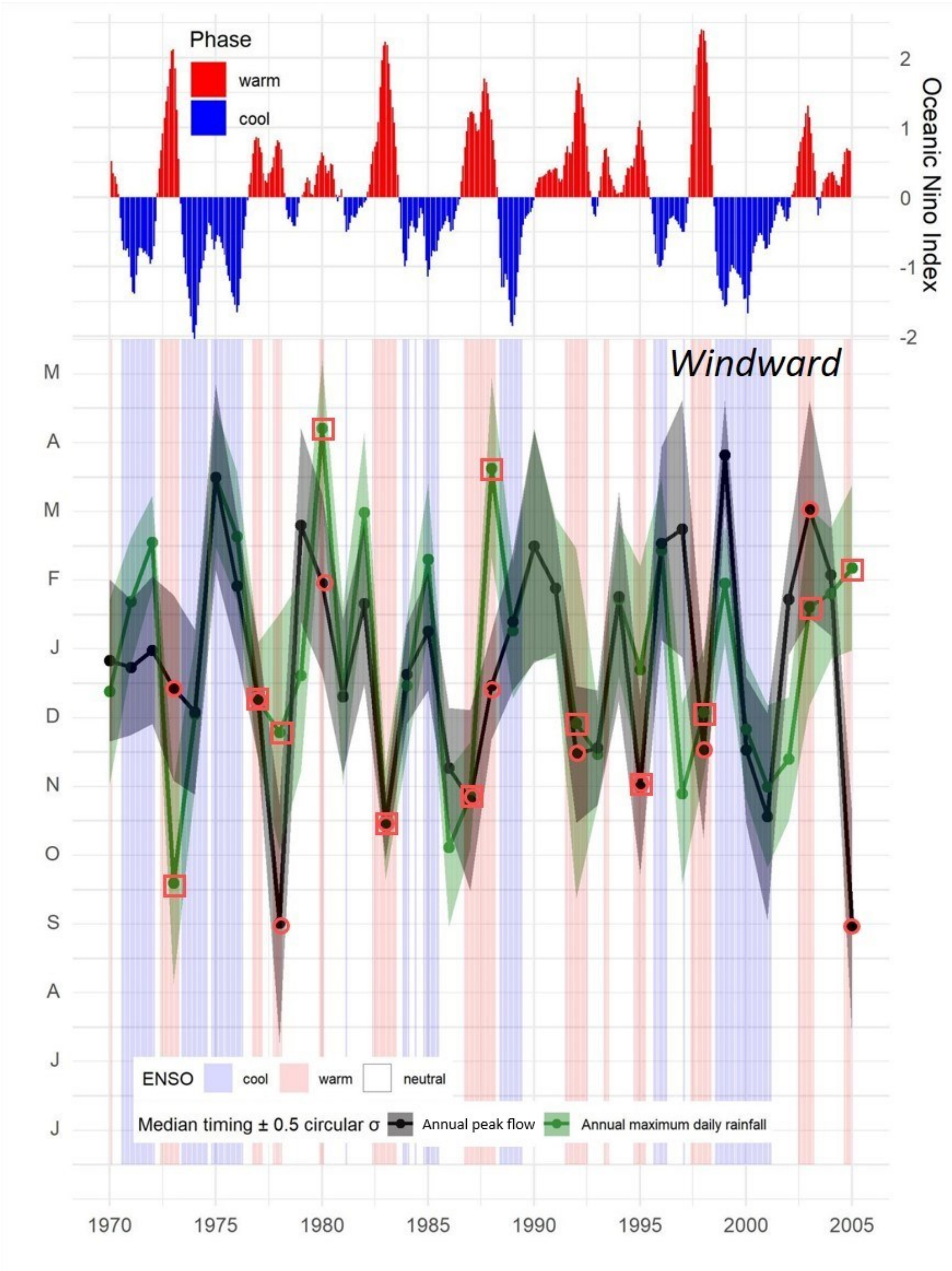

Figure 7 The occurrence time (median ± 0.5 circular deviation) of annual maximum daily rainfall (green line; n=34) and annual peak flow (black line; n=49) on the windward side with the ENSO phase shaded (red: warm phase; blue: cool phase, white: neutral). The y-axis indicates the months from June through May (bottom to top). Early occurrences under ENSO warm phase are indicated by red squares for annual maximum daily rainfall, and a red circle for annual peak flow. The Oceanic Nino Index (ONI) on the top indicates the strength of the ENSO from 1970 to 2005.